Diamond & Related Materials 56 (2015) 6–12

Contents lists available at ScienceDirect

Diamond & Related Materials

journal homepage: www.elsevier.com/locate/diamond

Surface Brillouin scattering on annealed ion-implanted CVD diamond

I. Motochi [a,*], S.R. Naidoo [a], B.A. Mathe [a], R. Erasmus [a], E. Aradi [a], T.E. Derry [a], E.J. Olivier [b]

[a] Materials Research Institute, DST-NRF Centre of Excellence in Strong Materials (CoE-SM), School of Physics, University of the Witwatersrand, Private bag 3, Wits 2050, Johannesburg, South Africa
[b] Centre for HRTEM, Nelson Mandela Metropolitan University, P.O Box 77000, Port Elizabeth 6031, South Africa

ARTICLE INFO

Article history:
Received 15 January 2015
Received in revised form 23 March 2015
Accepted 26 March 2015
Available online 3 April 2015

Keywords:
Ion implantation
Surface Brillouin scattering
Acoustic waves

ABSTRACT

Single crystal <100> diamond samples were implanted with a total fluence of 1.5×10^{16} ions/cm^2 at single energy of 150 keV using carbon ions. This implantation fluence created a damage density that would not restore the diamond structure after annealing. Surface Brillouin scattering studies show that the elastic properties of the highly damaged diamond layer starts to transit from diamond-like to amorphous carbon state at an annealing temperature of 500 °C. The amorphous carbon layer is shown to have a sound velocity (elastic properties) similar to those reported for tetrahedral amorphous carbon (ta-C). Raman spectroscopy, EELS and HRTEM has been used in conjunction with the SBS data to monitor the changes in the carbon implanted diamond at different annealing temperatures.

1. Introduction

Unlike the other group IV semiconductors, i.e., Si and Ge, ion implantation in diamond is challenging for application in semiconductor device construction. The tight bonding of the carbon atoms in the sp^3 hybridization, metastability of diamond and its vast difference in temperature with regards to the mobility of vacancies and interstitials act as stumbling blocks when using ion implantation and annealing to trap impurity atoms for *n* and *p* type doping [1].

Ion implantation causes structural changes in the sub-surface region in a material. The damage in diamond due to ion implantation and subsequent thermal treatment has been extensively studied [2–5]. It has been shown that ion implanted diamond with ion energies >10 keV to fluences above a damage threshold of $4–6 \times 10^{22}$ vac/cm^3, which is a simulated damage using TRIM irrespective of the implanted ion [6], will result in the collapse of the implanted region to an amorphous carbon. Subsequently annealing to temperature above 600 °C results in the damaged region evolving to a moderately graphitic layer. This region can be etched by boiling the diamond in an oxidizing acid solution or in an O_2 plasma environment. This approach has been used to lift off thin diamond layers and can be useful in ion beam patterning and machining of diamond [7]. The damaged layer after implantation and annealing apart from having graphitic carbon, also has amorphous carbon in the sp^n form where $n = 1, 2, 3$. This is in contrast with other group four elements (Si, Ge and Sn) single crystals which are isovalent with respect to carbon where ion implantation above the damage threshold results in amorphous sp^3 region [8,9].

This study investigates and reports changes in carbon ion implanted diamonds from observations made primarily using surface Brillouin spectroscopy (SBS). The observed results in SBS are compared with results obtained using Raman spectroscopy. Raman spectroscopy is a well established technique for studying structural changes of carbonaceous materials [10,11]. Furthermore, this information is correlated with electron energy loss spectroscopy (EELS) and high resolution transmission electron spectroscopy (HRTEM) measurements.

The extent of the damage induced by the carbon ions was theoretically estimated using the quantum Monte Carlo simulation program, SRIM2008 [12] using a displacement energy of 45 eV for the carbon in the diamond lattice (Fig. 1). The simulated damage density lies close to the damage threshold near the surface for the implanted fluence of 1.5×10^{16} ions/cm^2. It is observed that the damage profile gradually rises from the surface and reaches a maximum towards the tail end of the implanted range then abruptly falls off.

2. Experimental

The samples used were CVD single crystal diamond plate purchased from Element Six, of dimensions $3.0 \times 3.0 \times 0.5$ mm^3 with the 3.0×3.0 mm^2 polished faces oriented in {100}. The surface roughness of the polished faces was <30 nm as specified by the supplier. The implants were performed using a Varian 200-20A2F ion implanter at iThemba LABS, Gauteng, South Africa. The implantations were performed on one polished face at room temperature on samples tilted at about 7°. The ion beam was uniformly scanned over the sample surface with a beam current of $\approx 1.0\ \mu$A/cm^2. The low current minimized the effect of beam heating during implantation. The samples were implanted with single energy of 150 keV to a total fluence of 1.5×10^{16}

* Corresponding author.

http://dx.doi.org/10.1016/j.diamond.2015.03.022
0925-9635/

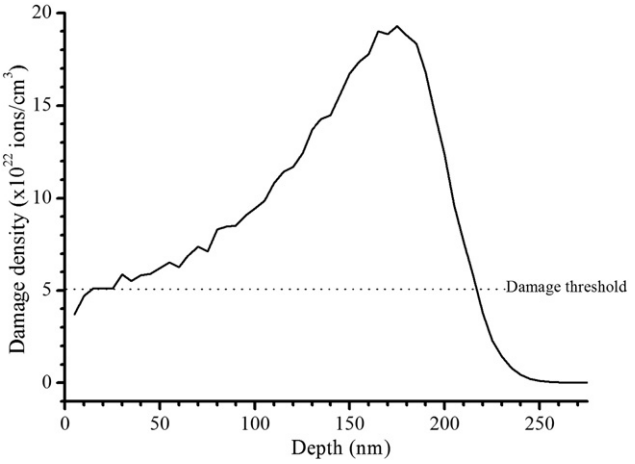

Fig. 1. Ion implantation scheme as implemented in SRIM2008. Carbon ions of fluence 1.5×10^{15} ions/cm^2 and displacement energy of 45 eV were used in the simulation.

ions/cm^2. Ion implantation caused visible optical changes in the samples observed as variation in transmission discussed in Section 3.1.

Isochronal annealing was done using the Carbolite Eurotherm 2416 furnace. Annealing temperatures were 200 °C, 400 °C, 500 °C, 600 °C, 800 °C, 1000 °C and 1200 °C in an inert Ar environment. A quartz glass tube that was held horizontally in the usual ceramic furnace tube (see Fig. 2) allowed for horizontal 'shoot in' of sample after pre-heating the furnace to a desired temperature. The quartz glass tube was purged for 15 min while the furnace temperature was ramping up to the desired annealing temperature. Once the dwell point was reached, the furnace was left to stabilize for at least 10 min. The sample was then introduced and annealed for 30 min. At the end of annealing time, the sample was quickly withdrawn from the heating zone by pulling away the quartz glass tube. It was then cooled in the continuous Ar gas flow until the temperature at point C was less than 100 °C. This was measured using thermocouple probe placed in such a way that it was in contact with the quartz tube at section C.

The sample was introduced by dropping it through funnel B then suddenly increasing the flow rate of the gas, "shooting it in" into the annealing section C, by an impulsive force. It was prevented from flying past this region by the perforated tube at D. The perforations also enable the exiting of the Ar gas from the annealing chamber. The gas flow rate is then gently reduced while monitoring the rotameter at A to ensure that the supply is never completely cut off. Gas flow is kept continuous throughout the purging, annealing and cooling processes. During this annealing process, the temperature of the sample is raised to a predefined set point in a small time interval of less than a second. The changes measured are therefore due to that particular temperature.

SBS and Raman measurements were taken after every anneal process. One such set of measurements were called a cycle. The same sample was annealed at a higher temperature and the cycle repeated. Raman measurements were done in backscattering using the 514.5 nm single laser mode. Like for Raman measurements, the SBS probing beam source was from an Ar^+ laser tuned on a 514.5 nm single mode line. SBS is the inelastic scattering of light by thermally excited phonons by dynamical modulation of the dielectric function of the medium (the elasto-optic effect) and/or dynamic corrugation of the surface (the surface ripple). A Brillouin scattering measurement involves illumination of the specimen by monochromatic laser light and analyzing the spectrum of the scattered light. In this study, a plane polarized light of ≈ 400 mW was produced at the source. The travel distance, reflections at mirrors and presence of an acousto-optic modulator (AOM) reduces the beam intensity to <100 mW on the sample. This is good enough to ensure minimal heating that does not affect the sample in any significant way. A scattered solid cone of light from the sample was collimated and focused onto the analyzer by means of mirrors and lenses. The scattered light was analyzed by a 3 + 3 pass Sandercock type tandem Fabry–Pérot interferometer described in [13]. The Krüger geometry [14] in backscattering mode was used to interpret the SBS data as both direct and indirect scattering mechanisms can be observed when the ion damaged diamond is still relatively transparent and the free polished surface at the opposite side of the implanted layer was held in position against a flat reflective aluminum plate. When the damaged region becomes semi-opaque after annealing at temperatures above 500 °C, then it can be interpreted that both the surface ripple mechanism and direct scattering from the bulk occur in the ion damaged and annealed layer.

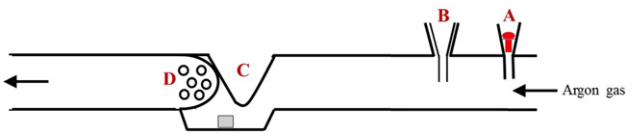

Fig. 2. A longitudinal cross-section of the modified glass tube used for annealing.

3. Results and discussions

3.1. SBS results

In Fig. 3, a consideration of the observed modes for both pristine diamond and C^+ implanted sample measured under the same scattering geometry shows no observable difference in frequency shift position of the implanted sample with respect to the pristine diamond. From Fig. 3, and subsequently in Fig. 4, the annealed diamond spectra up to 400 °C do not show any significant new features when compared to the pristine diamond. As shown in Section 3.3, the implanted region of width ≈240 nm sits on pristine diamond. Transmission measurements showed that pristine diamond transmits 69.3% of the 514.5 nm light. The transmission reduced to 15.8% for the as-implanted and anneal temperatures of up to 500 °C. In relation to SBS data, it is our view that the implanted region at the annealing cycles below 500 °C is not optically distinct from the pristine diamond below, and thus the elasto-optic scattering mechanism is unable to yield information specific to the implanted region at these lower annealing temperatures for the

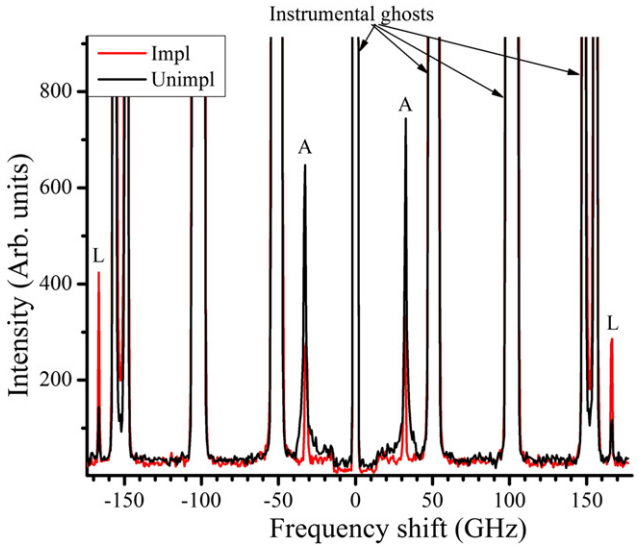

Fig. 3. SBS spectra recorded at 45° incidence for both the as-implanted and pristine diamond. The peaks labeled L (167 GHz) are bulk longitudinal modes due to direct elasto-optic scattering and the peaks labeled A (33 GHz) are due to indirect scattering via the Krüger scattering geometry [14] corresponding to transverse modes of the two samples. Instrumental ghosts are transmission peaks that are a function of the instrument and are useful in calibrating the spectrometer.

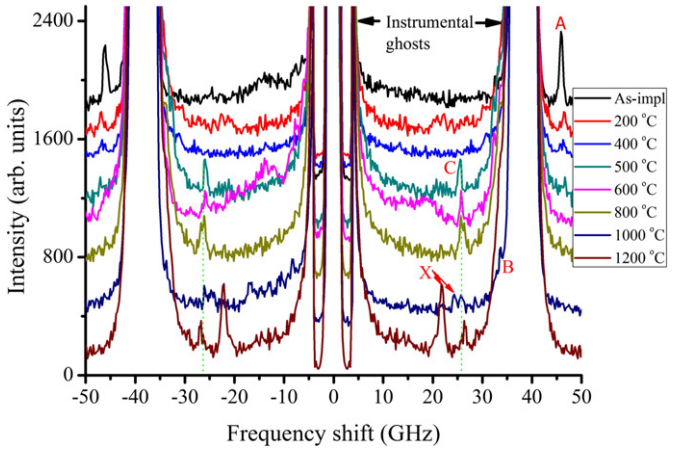

Fig. 4. SBS spectra for the C ion implanted diamond at different annealing temperatures, incident angle at 70°. Spectra displaced for clarity.

set-up used in this study. Measurements conducted after annealing at 600 °C show a drop in transmission to about 5%, and further drops to below 1% after anneal temperatures of 800 °C and above. These low values of transmission indicate that the annealed region has become increasingly opaque and therefore the ripple scattering mechanism [15] becomes predominant, hence the evolution of the surface modes at 1000 °C, observed in Fig. 4 and further analyzed in Fig. 5.

The SBS spectra after the different annealing cycles are shown in Fig. 4. Four distinct modes, labeled A, B, C and X appear in the spectral range 50 GHz. In our case, the focus was on a smaller spectral range up to ±50 GHz in order to observe phonons originating from the softer damaged layer as the annealing temperature was increased. At the lower annealing temperatures <500 °C, peak A was observed. There was a gradual reduction in peak A up to 500 °C anneal. It was observed at ≈ 46.2 GHz for an incident angle $\theta_i = 70°$, that a similar spectrum was obtained for an incidence angle of 80° with this peak observed at 48.6 GHz. With the aid of additional angle dependency measurements at $\theta_i = 50°$ and 60°, it was observed that peak A scales with $\sin\theta_i$, hence exhibiting a surface acoustic wave (SAW)-like characteristic, whose sound velocity was calculated using the following equation:

$$v_{saw} = \frac{\nu\lambda_0}{2\ \sin\theta_i}, \tag{1}$$

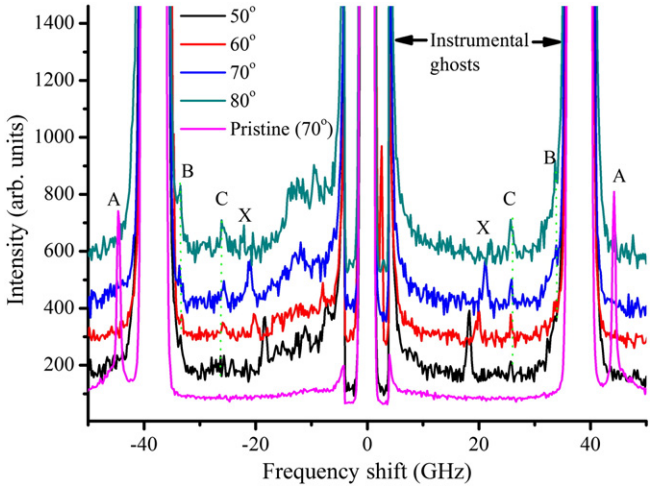

Fig. 5. SBS spectra for the implanted diamond after annealing at 1200 °C, incident angles varied between 50–80° while maintaining the same wavevector. Spectra are displaced for clarity. Pristine (70°) is the spectrum obtained from pristine diamond from light incident at 70°.

where ν is the frequency shift, λ_0 is the wavelength of the incident laser beam and θ_i is the angle of incidence that the beam makes normal to the sample's surface.

An analysis of the scattering geometry using the Krüger backscattering geometry explained in [16] shows that peak A is a bulk transverse mode probed by indirectly scattered photons as a result of the presence of a back reflective aluminum surface. Therefore, using Eq. (1), the velocity of peak A was obtained as ≈ 12,670 m/s, thus giving a C_{44} = 565 GPa. This is very close to 571 ± 0.3 GPa measured by Nakamura et al. [17] on CVD diamond, 577.4 GPa of Grimsditch and Ramdas [18] and slightly more than that of 541 ± 22 GPa of Jiang et al. [19] on polycrystalline CVD diamond.

Peaks B and C appeared after annealing at 500 °C. They remain visible after each subsequent anneal up to the highest anneal temperature of 1200 °C. Within the limits of experimental error, peaks B and C were observed to neither change from their position at higher anneal temperatures nor at different angles of incidence after the same anneal temperature. These two peaks appear to be related to bulk elastic modes of the damaged layer or they could be pseudo-surface acoustic wave (pSAW) modes induced by the influence of the gradually developing, increasingly opaque annealed implanted layer. Due to the related complexity of the scattering environment and the material changes under the annealing conditions, the authors noted that peaks B and C which are being reported for the first time for such an implanted diamond system, require further investigations to be fully understood. However, the fact that these peaks appear not to shift in position for increasing annealing temperatures could possibly indicate that the implanted diamond region has a fairly rigid phase which only changes drastically after annealing at 1000 °C, as shown by the formation of a new mode X in Fig. 4. In the context of this paper we investigate the properties of peak X since it will give insight into the elasticity of the near-surface region under study utilizing a well-established ripple scattering mechanism of the now opaque layer.

Peak X appears after 1000 °C anneal. It is also visible after annealing at 1200 °C and unlike peaks B and C, it shifted position to a lower frequency and it is dispersive. Peak X has the characteristic of a surface wave summarized in Fig. 5 and in Table 1. Generally, a surface wave travels parallel to the surface of an opaque material mediated by a light scattering mechanism known as surface ripple mechanism which relies largely on a reflective surface in order to realize sufficient scattering cross-sections. Thus the surface projected spectrum of long wavelength acoustic phonons of a homogenous semi-infinite body for a given surface phonon wavevector is the combination of a *discrete* (low frequency) set and a *continuous* (high frequency) set. In the discrete part, peaks corresponding to true surface waves (surface bounded modes) show up: true surface resonances. In the discrete part, *the Rayleigh wave* is found [20].

Transmission measurements done on the samples after annealing at 1000 °C have shown that transmittance of light of wavelength 514.5 nm drops to below 1%. This leads us to conclude that the damaged region is an opaque thin layer in intimate contact with a pristine diamond

Table 1
Frequency shift of peak X with respect to angle of incidence. The values in square brackets are the corresponding velocities when peak X is treated as a surface wave.

Annealing temperature (°C)	Angle of incidence	Peak X position (GHz) [velocity (m/s)]
1000 °C	50	19.2 [6450]
	60	22.2 [6590]
	70	24.5 [6710]
	80	25.7 [6710]
1200 °C	50	16.9 [5680]
	60	19.6 [5820]
	70	22.0 [6020]
	80	23.0 [6010]

substrate. Peak X is therefore a surface mode of this ion-implanted and annealed region, whose velocity is calculated using Eq. (1).

The Rayleigh velocity obtained after 1000 °C (average, 6620 m/s) is higher than that obtained after 1200 °C (5880 ± 100 m/s) within the 2% error in measurements using SBS. This observation implies that there is softening in the layer between the 1000 and 1200 °C anneal. The observed surface velocity due to peak X, compares well with velocities of Rayleigh wave obtained for homogeneous and layered 70 nm ta-C layer each, that was measured by Pastorelli et al. [20] using SBS. Based on the Rayleigh velocities measured with respect to peak X, it is best to assume that the entire damaged region from the surface to about 230–250 nm becomes an amorphous/graphitic layer whose properties resemble that of ta-C, as evidenced by the studies reported in Section 3.3.

3.2. Raman spectroscopy results

All Raman spectroscopy measurements were carried out on a Jobin-Yvon T64000 Raman spectrometer. After each annealing step described earlier, Raman measurements were made on the implanted diamond. The results are shown in Fig. 6.

The diamond's Raman active mode at 1332 cm^{-1} is present on the as-implanted diamond and lattice damage from Raman active distortions of the lattice appears at about 1540 cm^{-1}. After annealing, the 1332 cm^{-1} peak diminishes gradually from the as-implanted to 500 °C and slightly visible after the 600 °C anneal. The appearance of a broad peak, the D peak becomes more prominent after annealing at 500 °C and becomes more distinct after annealing at 1000 °C and the damaged layer has distinct D and G peaks after annealing at 1000 °C. The D peak is centered at about 1350 cm^{-1} while the G peak is at 1590 cm^{-1}. The narrowing of the G peak reflects an increase in graphitic order within the implanted layer [21]. Fig. 7 shows shifts in the G peak position as a function of annealing temperature.

Furthermore, Raman measurements with different wavelengths (514.5 and 785 nm) after the 1200 °C showed no dispersion in the G peak position. As discussed by Ferrari and Robertson [22], the G and D peaks are due to sp^2 bonding. The G peak is due to the bond stretching of all pairs of the sp^2 atoms in both rings and chains while the D peak is due to the breathing modes of rings. It is worth noting that for the implantation conditions and fluence used in this study the G peak in the Raman spectra after implantation is a broad peak centered around 1540 cm^{-1}. For low fluence implants under the same conditions the G peak is a narrower peak centered around 1638 cm^{-1} [23,24]. This Raman peak has been identified as the split <100> interstitial. The defect consists of two central carbon atoms that are sp^2 bonded each having a nonbonded π-orbital normal to the plane containing the sp^2 bonds [25]. For the implantation conditions used in this experiment the Raman data suggests that the sp^2 bonded carbon is not from isolated point defects but possibly from scattered sp^2 clusters which are small and are formed during the implantation process for high fluence implantation and the ion energies of the order of 10–500 keV. Dispersion of the sp^2 Raman signature using visible light shows that there is little order in the sp^2 clusters. Upon thermal annealing the sp^2 clusters aggregate and form nanocrystalline graphite, which is evident in the lack of dispersion of the G peak after annealing at 1000 °C.

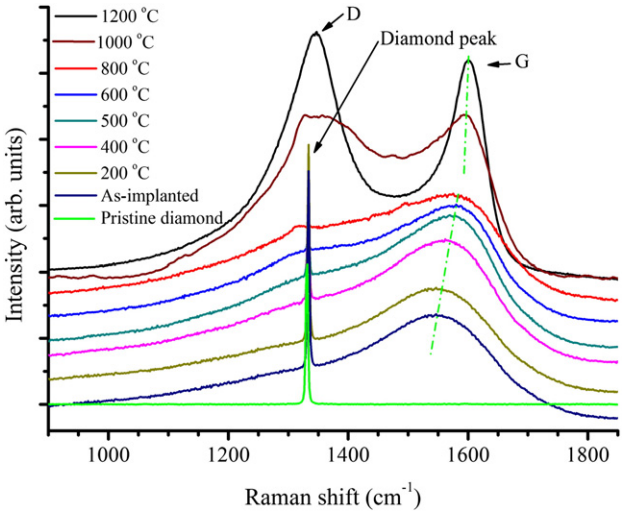

Fig. 6. Raman spectra for the C ion implanted diamond at different annealing temperature. Spectra displaced for clarity.

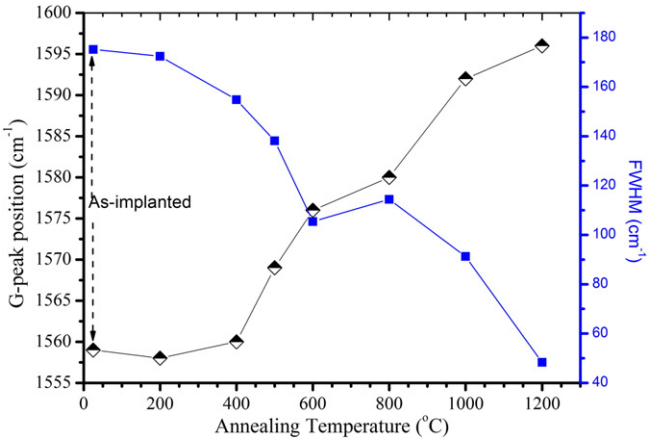

Fig. 7. Change in G peak position and FWHM using Gaussian fit for C implanted diamond as a function of annealing temperature. The peak positions are the Gaussian fits of the experimental data. The solid line is just a guide to the eye.

3.3. EELS and HRTEM results

A single crystal CVD diamond plate similar to the sample used earlier was implanted with C ions at single energy of 150 keV and total fluence of 1.5×10^{16} ions/cm^2. It was then broken into smaller pieces. Different pieces were annealed at temperatures between 200 °C and 1000 °C for 20 min in flowing argon environment. Though the annealing cycle was different from that used to acquire SBS and Raman data and this partial data set forms part of another study to be published elsewhere, the information obtained is useful in the overall interpretation and comparison of data. In this case each piece was annealed once at a specific temperature (say one piece at 200 °C, another at 400 °C, etc.), unlike previously where the sample was annealed at 200 °C, then after SBS and Raman measurements, the same sample was annealed at 400 °C, etc. From each annealed piece, FIB sections were prepared using a FEI Helios Nanolab 650. Then TEM analysis was done using a double aberration corrected JEOL ARM 200 F fitted with a Gatan GIF Quantum ERS 965 with dual EELS capability as detailed in [26]. A beam current of 68 pA and probe size of ≈ 0.1 nm was used. The convergence and acceptance angles of 24–27 Mrad and 70–100 Mrad, respectively were used. By using STEM-EELS spectrum imaging, the bonding environment of the as-implanted layer and subsequently annealed profiles was mapped. The disordered carbon was mapped using the characteristic pi bonding pre-edge for disordered carbon present at 284 eV energy loss for the C K-edge using an energy window of 4 eV. The diamond signal was mapped by using a multiple linear least square (MLLS) fitting of the spectrum image area using a reference signal of diamond. The produced maps are shown in Fig. 8a. By scanning across the entire region of implanted range on each annealed piece, the percentages of disorder in carbon bonds and diamond bonding in the region was mapped. The selected area diffraction (SAD) pattern was taken over the width of the amorphous implanted zone so as to exclude as much as possible the diamond material at the near surface and the diamond substrate beyond the end of range, this is shown in Fig. 9.

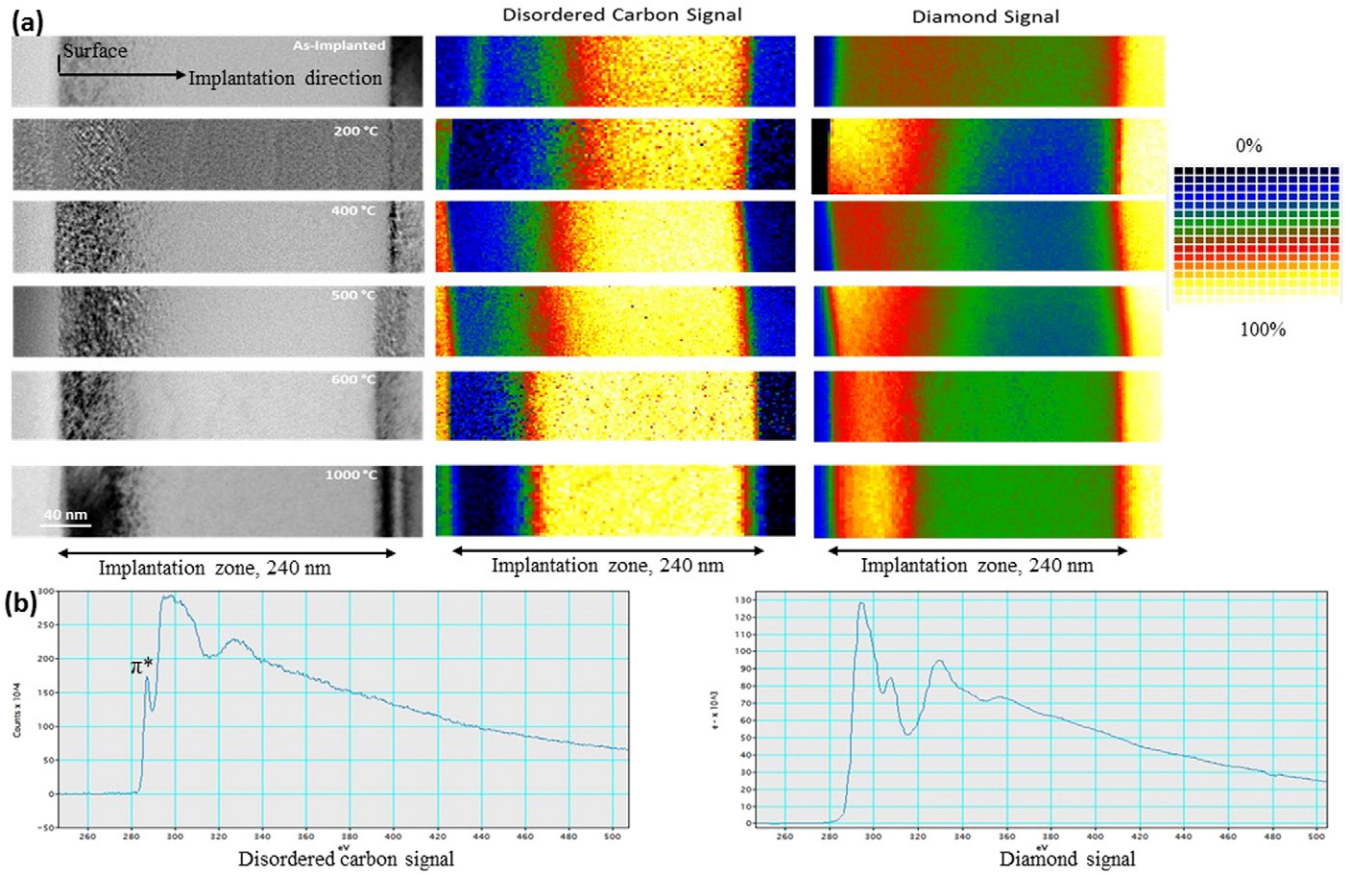

Fig. 8. (a) Bright field micrographs of C ion implanted and annealed at the temperatures shown with corresponding STEM-EELS spectrum images shown alongside. A very thin diamond layer occupies the top part of the ≈ 240 nm implantation zone. Just beneath this layer, an amorphous layer that was evolving due to heat treatment seems to saturate after annealing at 1000 °C. The grid to the right shows the percentage of disorder/ diamond in the implantation zone. (b) Core loss EEL spectrum of the carbon k-edge used in mapping the middle and right column EELS spectrum of the implanted layer.

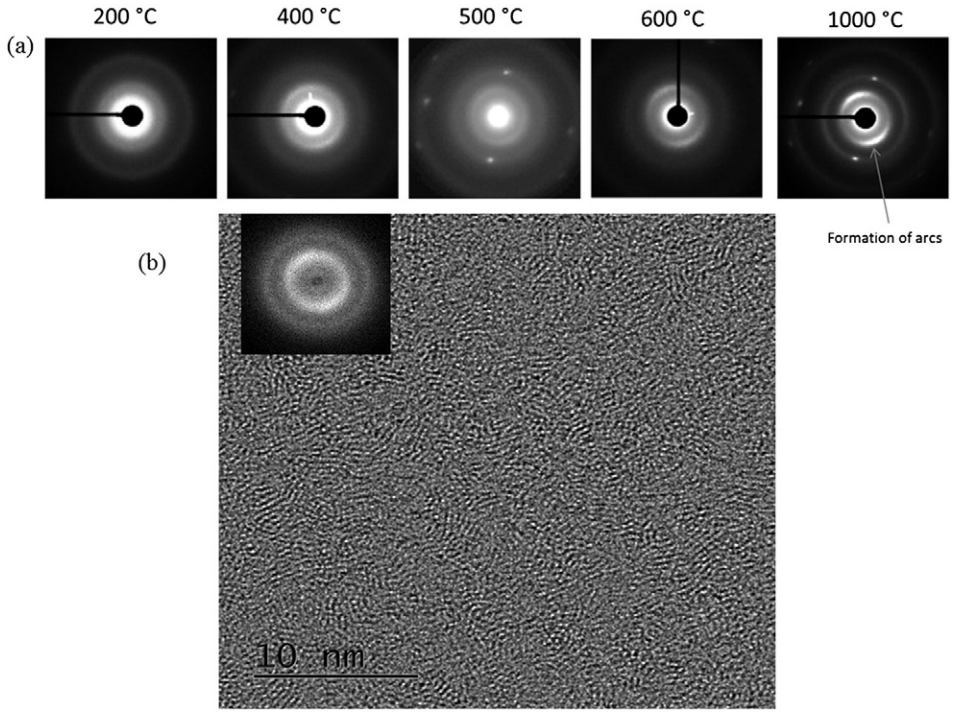

Fig. 9. (a) SAD patterns from implanted zone at different annealing temperatures. (b) HRTEM image of the damaged zone after 1000 °C anneal.

It is observed that implanted zone consists of largely an amorphous region of ≈250 nm in width. However, some diamond crystallinity was maintained at the near surface region after implantation. Annealing of the implanted zone led to a reduction in the width of the near surface diamond region and consequently an expansion in the disordered or amorphous-like carbon region. Sharpness of the boundary at the diamond–amorphous layer interface near the surface improved as the annealing temperature increased (Fig. 8a). Evidence for the alignment of graphitic basal planes was found with an increase in annealing temperature as determined by SAD and HRTEM shown in Fig. 9. This can be seen due to the presence of the arcs in the SAD pattern and alignment of the basal planes in the HRTEM image. The lack of long range crystallinity in the graphitic carbon is also supported by the arcs observed in the SAD patterns which appear after annealing at 600 °C [26].

We compare the results summarized in the SBS spectra of Fig. 4 and the Raman spectra (Fig. 6), and corroborate them with the EELS and HRTEM measurements. It is observed that peak A, earlier identified as a bulk transverse wave of diamond was only visible at annealing regimes that also showed an intense first order diamond signal in Raman measurements. This could be due to the diamond near the surface as well as beyond the damaged region. There is a correlation between the SBS and Raman measurements determined by the opacity of the damaged layer as reported earlier in Section 3.1 on transmission of the 514.5 nm light as a function of annealing. This is shown by the decrease in the intensities of SHM mode in SBS and Raman diamond signal as the layer became more opaque. As the disorder peak became more prominent after annealing at 500 °C as observed in Raman measurements, peaks B and C appeared in SBS measurements. These peaks appear after annealing at temperatures >500 °C when vacancies become mobile in diamond [4]. The annealing process associated with vacancy migration appears to be related to the clustering of the sp^2. A process similar to Ostwald ripening takes place where materials with lower formation energy are preferred hence more clusters of sp^2 bonds form at the expense of sp^3 bonded ones in the damaged region. The alignment of the basal planes of graphitic carbon is seen as arcs in the SAD pattern taken over the implanted range and is more clearly visible after annealing at 600 °C as seen in Fig. 8(a). After the 200, 400 and 500 °C anneals the SAD pattern which are rings indicates that the damaged region is amorphous. The SBS spectra only showed additional peaks after annealing at 500 °C which must be from direct backscattering from the phonons in the ion implanted and annealed layer. Annealing above 500 °C appears to be accompanied with the clustering and closer proximity of the graphitic carbon in the implanted region.

In SBS a new material in which sound propagates slower than diamond was detected as peaks B and C and later as X when the reflectivity of the surface is good enough. The HRTEM image shown in Fig. 9(b) shows that the layer consists of bent carbon basal planes with no long range order and amorphous carbon which can consist of sp^2 and sp^3 bonded carbon. Reflectivity of the damaged layer improves as the boundary at the diamond-damaged region becomes sharper (see Fig. 8 in [26]). In EELS data, the boundary is observed to become sharper after higher annealing temperature of 600 °C, and greatly improved at 1000 °C. The EELS and HRTEM results show that for C implanted diamond beyond a critical threshold, the diamond is irreversibly damaged and solid epitaxial regrowth does not take place in diamond. This could be the reason why a sharp interface forms between the diamond and amorphous region. We also observe that in the EELS spectrum image map there is a thin diamond layer that remains intact at the surface, such strain distorted diamond has also been observed in He ion implanted diamond [27]. This was not observed in the Raman spectra, and this could be due to the difference in the annealing cycle and possibly the shorter time that the diamond pieces were annealed for in the HRTEM/EELS study. It could also be that if there is a thin layer of diamond at the surface in the diamond used for the Raman study, that the diamond Raman line is overwhelmed under the D peak due to the large scattering cross-section for the D band in Raman scattering using visible light. In the SBS spectra after annealing above 500 °C, the peak due to indirect scattering labeled A reduces in intensity and is not visible after annealing at temperatures above 600 °C. If we take that there is a diamond layer at the surface that remains, as the EELS spectrum image shows (Fig. 8), then it can be argued that the scattering path length of the light from the diamond structure at the surface (approximately 50–60 nm) reduces the number of elasto-optic scattering events that occur via the indirect scattering mechanism, hence the lack of signal observed.

Peak X in SBS spectra of Fig. 4, observed after annealing at 1000 °C coincides with appearance of distinct peaks D and G in the Raman measurements. Notably, peak X reported in SBS measurements appears after the 1000 °C anneal, which corresponds to the damage profile that has a sharp boundary on the surface side observed by electron microscopy. Basing on the trend at 800 °C and 1000 °C, the boundary would only get sharper after annealing at 1200 °C, which would explain the increased intensity of peak X in SBS. From these observations, peak X is identified as a surface mode of the amorphized damaged region which consists of a network of carbon (sp^n, $n = 1,2,3$) with some of the sp^2 in the form of *nc*-graphite. The formation of arcs in the SAD in Fig. 9(a) is from the bent graphitic regions seen in Fig. 9(b) [26]. The amorphized region is characterized by a softer surface mode velocities of ≈ 5700–6710 m/s for the range of incidence angles probed. This is far less than the Rayleigh velocity of diamond reported by Djemia et al. [28] of 10,800 ± 300 m/s on polycrystalline diamond measured using SBS but much closer to velocities of 5300–6800 m/s reported by Pastorelli et al. [20] for homogeneous and layered ta-C measured using SBS.

4. Conclusion

This study, using SBS has shown the transition in elastic properties that occur as C^+ implanted CVD diamond is annealed. The transition characterized by appearance of sound modes that show a softer layer were observed after annealing the sample at 500 °C. This observation is being reported for the first time to the best of our knowledge. The SBS results have been corroborated by Raman, EELS and HRTEM measurements. These studies have shown a correlation between the structural changes and elastic properties that occur in ion-implanted and annealed diamond. SBS did not show reduction in the velocity of the diamond lattice related peak (peak A) as annealing temperature increases, it rather showed a transition from a hard to a softer material, shown by appearance of slower acoustic modes B, C and X. The velocity of the Rayleigh mode obtained after annealing at 1000 °C is within the range of reported Rayleigh velocities of the ta-C.

Fruitful discussions with Prof. Arthur Every of the University of the Witwatersrand is hereby acknowledged. The support of the DST-NRF Centre of Excellence in Strong Materials (CoE-SM) towards this research is hereby acknowledged. Special thanks for financial support from African Laser Centre (ALC) for the first author, Project number LHIJ500 Task ALC S100.

Prime novelty statement

The study has shown the for the first time the correlation between structural change of ion-implanted diamond and its effect on elasticity due to heat treatment using surface Brillouin scattering as the principal technique. The results are corroborated with observations made from Raman, HRTEM and EELS measurements.

References

[1] T. Vogel, J. Meijer, A. Zaitsev, Highly effective p-type doping of diamond by MeV-ion implantation of boron, Diam. Relat. Mater. 13 (2004) 1822–1825, http://dx.doi.org/10.1016/j.diamond.2004.04.005.

[2] R. Spits, T. Derry, J. Prins, Annealing studies on ion implanted diamond, Nucl. Inst. Methods B 64 (1992) 210–214, http://dx.doi.org/10.1016/0168-583X(92)95467-6.

[3] R. Kalish, A. Reznik, S. Prawer, D. Saada, J. Adler, Ion-implantation-induced defects in diamond and their annealing: experiment and simulation, Phys. Status Solidi A 174 (83) (1999) 83–99, http://dx.doi.org/10.1002/(SICI)1521-396X(199907)174:1<83::AID-PSSA83>3.0.CO;2-3.
[4] J. Prins, T. Derry, Radiation defects and their annealing behaviour in ion-implanted diamonds, Nucl. Inst. Methods B 166–167 (2000) 364–373, http://dx.doi.org/10.1016/S0168-583X(99)01190-8.
[5] A. Collins, I. Kiflawi, The annealing of radiation damage in type Ia diamond, J. Phys. Condens. Matter 21 (2009) 364209, http://dx.doi.org/10.1088/0953-8984/21/36/364209 (8 pp.).
[6] D. Hickey, K. Jones, R. Elliman, Amorphization and graphitization of single-crystal diamond-a transmission electron microscopy study, Diam. Relat. Mater. 18 (2009) 1353–1359, http://dx.doi.org/10.1016/j.diamond.2009.08.012.
[7] M.P. Ray, J.W. Baldwin, T.I. Feygelson, J.E. Butler, B.B. Pate, Note: laser ablation technique for electrically contacting a buried implant layer in single crystal diamond, Rev. Sci. Instrum. 82 (2011) 056105, http://dx.doi.org/10.1063/1.3595678.
[8] C.A. Londos, E.N. Sgourou, D. Timerkaeva, A. Choneos, P. Pochet, V.V. Emtsev, Impact of isovalent doping on radiation defects in silicon, J. Appl. Phys. 113 (2013) 113504, http://dx.doi.org/10.1063/1.4821116.
[9] G. Gaidar, Investigation of the influence of isovalent impurity of silicon and γ-irradiation (^{60}Co) on electrophysical parameters of *n*-ge, Semicond. Phys. Quant. Electron. Optoelectron. 17 (1) (2014) 25–28.
[10] J. Hunn, S. Withrow, C. White, D. H. Jr., Raman scattering from MeV-ion implanted diamond, Phys. Rev. B 52 (1995) 8106–8111, http://dx.doi.org/10.1103/PhysRevB.52.8106.
[11] A. Ferrari, J. Robertson, Interpretation of Raman spectra of disordered and amorphous carbon, Phys. Rev. B 61 (2000) 14095–14107, http://dx.doi.org/10.1103/PhysRevB.61.14095.
[12] J. Ziegler, J. Biersack, M. Ziegler, The Stopping and Range of Ions in Matter, Ultrasonics, Chester Maryland 21619 USA, 2008. 11–17.
[13] R. Mock, B. Hillebrands, R. Sandercock, Construction and performance of a Brillouin scattering set-up using a triple-pass tandem Fabry–Perot interferometer, J. Phys. E Sci. Instrum. 20 (1987) 656–659, http://dx.doi.org/10.1088/0022-3735/20/6/017.
[14] J. Krüger, J. Embs, J. Brierly, J. Rioboo, A new Brillouin scattering technique for the investigation of acoustic and opto-acoustic properties: application to polymers, J. Phys. D. Appl. Phys. 31 (15) (1998) 1913–1917, http://dx.doi.org/10.1088/0022-3727/31/15/021.
[15] J.D. Comins, A.G. Every, P.R. Stoddart, X. Zhang, J.C. Crowhurst, G.R. Hearne, Surface Brillouin scattering of opaque solids and thin supported films, Ultrasonics 38 (2000) 450–458, http://dx.doi.org/10.1016/S0041-624X(99)00199-7.
[16] M. Beghi, F.D. Fonzo, S. Pietralunga, C. Ubaldi, C. Bottani, Precision and accuracy in film stiffness measurement by Brillouin spectroscopy, Rev. Sci. Instrum. 82 (2011) 053107, http://dx.doi.org/10.1063/1.3585980.
[17] N. Nakamura, H. Ogi, M. Hirao, Elastic constants of chemical-vapor-deposition diamond thin films: resonance ultrasound spectroscopy with laser-Doppler interferometry, Acta Mater. 52 (2004) 765–771, http://dx.doi.org/10.1016/j.actamat.2003.10.012.
[18] M. Grimsditch, A. Ramdas, Brillouin scattering in diamond, Phys. Rev. B 11 (8) (1975) 3139–3148, http://dx.doi.org/10.1103/PhysRevB.11.3139.
[19] X. Jiang, J. Harzer, B. Hillebrands, C. Wild, P. Koidle, Brillouin light scattering on chemical-vapor-deposited polycrystalline diamond: evaluation of the elastic moduli, Appl. Phys. Lett. 59 (9) (1991) 1055–1057, http://dx.doi.org/10.1063/1.106343.
[20] R. Pastorelli, A.C. Ferrari, M.G. Beghi, C.E. Bottani, J. Robertson, Elastic constants of ultrathin diamond-like carbon films, Diam. Relat. Mater. 9 (2000) 825–830, http://dx.doi.org/10.1016/S0925-9635(99)00245-9.
[21] D. McCulloch, S. Prawer, The effect of annealing and implantation temperature on the structure of c ion-beam-irradiated glassy carbon, Appl. Phys. Lett. 78 (5) (1995) 3040–3047, http://dx.doi.org/10.1063/1.360054.
[22] A. Ferrari, J. Robertson, Resonant Raman spectroscopy of disordered, amorphous, and diamondlike carbon, Phys. Rev. B 64 (2001) 075414, http://dx.doi.org/10.1103/PhysRevB.64.075414.
[23] J. Orwa, K. Nugent, D. Jamieson, S. Prawer, Raman investigation of damage caused by deep ion implantation in diamond, Phys. Rev. B 62 (2000) 5461–5472, http://dx.doi.org/10.1103/PhysRevB.62.5461.
[24] S. Prawer, I. Rosenblum, J.O. Orwa, J. Adler, Identification of the point defects in diamond as measured by Raman spectroscopy: comparison between experiment and computation, Chem. Phys. Lett. 390 (2004) 458–461, http://dx.doi.org/10.1016/j.cplett.2004.04.027.
[25] D. Hunt, D. Twitchen, M. Newton, J. Baker, T. Anthony, W. Banholzer, S. Varagali, Identification of the neutral carbon <100>-split interstitial in diamond, Phys. Rev. B 61 (2000-II) 3863–3876, http://dx.doi.org/10.1103/PhysRevB.61.3863.
[26] E. Nshingabigwi, T. Derry, S. Naidoo, J. Neethling, E. Olivier, J. O'Connell, C. Levitt, Electron microscopy profiling of ion implantation damage in diamond: dependence on fluence and annealing, Diam. Relat. Mater. 49 (8) (2014) 1–8, http://dx.doi.org/10.1016/j.diamond.2014.07.010.
[27] B.A. Fairchild, S.D. Rubanov, D.W.M. Lau, M. Robinson, I. Suarez-Matinez, N. Marks, A.D. Greentree, D. McCulloch, S. Prawer, Mechanism for amorphisation of diamond, Adv. Mater. 24 (2012) 2024–2029, http://dx.doi.org/10.1002/adma.201104511.
[28] P. Djemia, C. Dugautier, T. Chauveau, E. Dogheche, M. Barros, L. Vandenbulcke, Mechanical properties of diamond films: a comparative study of polycrystalline and smooth fine-grained diamonds by Brillouin light scattering, J. Appl. Phys. 90 (8) (2001) 3771–3779, http://dx.doi.org/10.1063/1.1402667.